RESEARCH ARTICLE

Design, synthesis, in vitro and in silico studies of novel Schiff base derivatives of 2-hydroxy-4-methoxybenzamide as tyrosinase inhibitors

Aida Iraji[1] [ID] | Zahra Panahi[2] [ID] | Najmeh Edraki[1] [ID] |
Mahsima Khoshneviszadeh[1] [ID] | Mehdi Khoshneviszadeh[1,2] [ID]

[1]Medicinal and Natural Products Chemistry Research Center, Shiraz University of Medical Sciences, Shiraz, Iran

[2]Department of Medicinal Chemistry, Faculty of Pharmacy, Shiraz University of Medical Sciences, Shiraz, Iran

Correspondence
Mehdi Khoshneviszadeh, Medicinal and Natural Products Chemistry Research Center, Shiraz University of Medical Sciences, Shiraz, Iran.
Email: m.khoshneviszadeh@gmail.com

Abstract

Due to the fact that tyrosinase is responsible for biosynthesis and regulation of melanins and browning food products, tyrosinase inhibitors can be favorable agents in cosmetics and medicinal industries. A series of novel 2-hydroxy-4-methoxybenzohydrazide were designed, synthesized, and their new application as tyrosinase inhibitors was also disclosed. Based on *in vitro* tyrosinase inhibitory assay, **4d** as the strongest inhibitor of tyrosinase with an IC_{50} value of 7.57 μM showed approximately 2.5-fold better inhibition than kojic acid as positive control followed by two compounds **4b** (IC_{50} = 8.19 ± 0.25 μM) and **4j** (IC_{50} = 8.92 ± 0.016) which displayed preferable tyrosinase inhibitory activity. Detailed investigations on the mechanism of action of the **4d** reported mix type of inhibition. More importantly, molecular modeling assessments proposed the ability of **4d** for potential interaction with Cu (metal)-His (residue) within tyrosinase active site. Overall, **4d** is a promising candidate for the development of anti-tyrosinase agents.

KEYWORDS

2-hydroxy-4-methoxybenzamide, kinetic study, molecular docking, synthesis, tyrosinase inhibitor

1 | INTRODUCTION

Melanins are the pigments responsible for hair and skin color. The abnormal accumulation of pigment in the body can cause hyperpigmentation problems and skin disorders including age spots, melasma, and melanoma (Loizzo et al., 2012). Tyrosinase (TYR) oxidoreductase enzyme (EC 1.14.18.1) widely distributed in microorganisms, humans, animals, and plants. TYR and other tyrosinase-like protein have an initial, and critical role in melanin synthesis and catalysis rate-limiting step of melanin biosynthesize (Zolghadri et al., 2019).

Tyrosinase hydroxylates monophenols compounds (e.g., l-tyrosine as precursor substrate) to o-diphenols (e.g., L-dopa as the second substrate) and catalyzes o-diphenols to the o-quinones (e.g., dopaquinone) (Hałdys & Latajka, 2019). Besides, the action of TYR has increased enzymatic browning reaction results in deteriorating food during commercial or domestic processing and storage (Singh et al., 2018). It seems that tyrosinase inhibitors (TYRI) could have potential applications in diverse areas of agriculture, cosmetics, and pharmaceuticals (Yuan et al., 2020). Different studies also confirmed the role of TYR in neurodegenerative and autoimmune disorders (Lavezzo et al., 2016; Neagu et al., 2018; Piechowska et al., 2019).

TYR is a tetrameric Cu-containing metalloenzyme belonging to the type-3 copper protein family. TYR composes two heavy subunits (H subunits) with around about 43 kDa and two light subunits of

Abbreviations: ^{13}C NMR, carbon-13 nuclear magnetic resonance; ^{1}H NMR, proton nuclear magnetic resonance; Ala, alanine; Arg, arginine; DMSO-d_6, deuterated dimethyl sulfoxide; His, histidine; L-dopa, L-dihydroxyphenylalanine; LGA, Lamarckian genetic algorithm; L-Tyr, L-tyrosinase; Lue, Lucine; Pro, proline; Val, Valine.

about 14 kDa (L subunits). In the TYR active site, two copper ions bound to three conserved essential histidine residues (Choi et al., 2015; Ismaya et al., 2011; Matoba et al., 2006).

2 | MATERIAL AND METHOD

2.1 | Chemistry

All reagents were purchased from commercial sources and were used without further. Solvents were procured from Merck and Samchane. Thin-layer chromatography (TLC) was performed on Silica gel 60 F254 coated plates (Merck) to check the purity of compounds. ^{1}H and ^{13}C NMR were recorded in Bruker NMR 500 and 125 MHz spectrophotometer. All the chemical shifts were reported as (δ) values (ppm). Melting points were determined by Gallenkamp melting point apparatus. FT-IR Perkin Elmer spectrophotometer was used. Mass spectra were obtained on the Agilent 7890A spectrometer at 70 eV.

2.1.1 | Synthesis of 2-hydroxy-4-methoxybenzohydrazide (2)

The methyl 2-hydroxy-4-methoxybenzoate (Compound **1**, 2 mmol) and hydrazine hydrate (3 mmol) were refluxed in ethanol (50 ml) for 4 h in the presence of the catalytic amount of acetic acid. The mixture was cooled and kept for 3–4 h at room temperature. The solid separated was filtered, dried and recrystallized from ethanol. The product was carefully checked by TLC (Khoshneviszadeh et al., 2013; Yazdani et al., 2019).

2.1.2 | General procedure for the synthesis of compounds (4a–j)

The final step was performed according to the reported literature. For this purpose, 2-hydroxy-4-methoxybenzohydrazide (Compound **2**, 1 mmol) was dissolved in 50 ml ethanol at room temperature. The reaction mixture was stirred for 10 min and different selected aldehyde (Compound **3**, 1.2 mmol) were added. After 12 h string at 50°C, the mixture was cooled to room temperature and filtered. The residue was recrystallized from ethanol to give the pure product. In the case of some compounds, they were purified using plate chromatography with EtOH/CHCl$_3$ as eluent (Iraji et al., 2018).

Synthesis of 2-hydroxy-4-methoxy-N′-(3-nitrobenzylidene) benzohydrazide (4a)

Yellow crystal; Yield: 60%; M.P: 260–264°C; ^{1}H NMR (500 MHz, DMSO-d_6) δ_H (ppm): 2.23 (s, 3H, CH$_3$), 7.71 (m, 2H, Ar-H), 8.08 (s, 1H, Ar-H) 8.10 (d, J = 7.6 Hz, 1H, Ar-H), 8.21 (dt, J = 7.7, 3.8 Hz, 2H, Ar-H), 8.42 (s, 1H, Ar-H), 8.48 (s, 1H, N=CH), 11.47 (s, 1H, OH), 11.62 (s, 1H, N-H); ^{13}C NMR (126 MHz, DMSO) δ_c (ppm): 19.7, 120.2, 120.3, 123.3, 123.5, 129.8, 132.2, 132.6, 135.6, 135.74, 139.6, 142.6, 147.6,

165.4, 171.7; MS (EI), m/z (%):151.0 (100), 166.0 (40), 315.0 (M$^+$, 15); I.R (KBr) υ_{max} (cm^{-1}): ArO-H: 3497, N-H: 3293, C-H-aromatic: 3093, C-H-aliphatic: 2970, C-H-aliphatic: 2927, C-H-aliphatic: 2840, C=O amide:1679, C=N:1643, N-O nitro:1523, N-O nitro: 1332, C=C aromatic:1477, CH$_3$:1387, C-N: 1289, C-O:1135.

Synthesis of 2-hydroxy-4-methoxy-N′-(4-nitrobenzylidene) benzohydrazide (4b)

Yellow crystal; Yield: 54%; M.P: 264–266°C; ^{1}H NMR (500 MHz, DMSO-d_6) δ_H (ppm): 3.81 (s, 3H, OCH$_3$), 6.51 (d, J = 2 Hz, 1H, H$_3$-2-hydroxy-4-methoxy-N′-methylenebenzohydrazide), 6.57 (dd, J = 8.8, 2.0 Hz, 1H, H$_5$-2-hydroxy-4-methoxy-N′-methylenebenzohydrazide), 7.91 (d, J = 8.8 Hz, 1H, Ar-H), 7.99 (d, J = 8.4 Hz, 2H, Ar-H), 8.30 (d, J = 8.6 Hz, 2H, Ar-H), 8.55 (s, 1H, CH=N), 11.98 (s, 1H, OH), 12.22 (s, 1H, NH); ^{13}C NMR (126 MHz, DMSO) δ_c (ppm): 54.9, 100.8, 105.98, 107.0, 123.5, 127.5, 129.3, 139.9, 145.1, 147.4, 161.5, 163.5, 164.8; MS (EI), m/z (%): 151.0 (100), 180.1 (47), 315.1 (M$^+$, 17); I.R(KBr) υ_{max} (cm^{-1}): ArO-H: 3331, N-H: 3321, C-H-aromatic: 3027, C-H-aromatic: 3016, CH-aliphatic: 2971, CH-aliphatic: 2931, C=O amide: 1656, C=N: 1593, C=C aromatic: 1553, C=C aromatic: 1491, N-H: 1511, CH$_3$: 1362, C-N: 1258, C-O: 1156, C-Cl: 847.

Synthesis of N′-(4-bromobenzylidene)-2-hydroxy-4-methoxybenzohydrazide (4c)

White crystal; yield: 57%; M.P: 224–227°C; ^{1}H NMR (500 MHz, DMSO-d_6) δ_H (ppm): 3.80 (s, 3H, OCH$_3$), 6.51 (s, J = 2.8 Hz, 1H, H$_3$-2-hydroxy-4-methoxy-N′-methylenebenzohydrazide), 6.56 (dd, J = 9.0, 2.8 Hz, 1H, H$_5$-2-hydroxy-4-methoxy-N′-methylenebenzohydrazide), 7.68 (q, J = 8.5 Hz, 4H, Ar-H), 7.90 (d, J = 8.9 Hz, 1H, H$_6$-2-hydroxy-4-methoxy-N′-methylenebenzohydrazide), 8.43 (s, 1H, CH=N), 11.85 (s, 1H, OH), 12.46 (s, 1H, NH); ^{13}C NMR (126 MHz, DMSO) δ_c (ppm): 54.9, 100.8, 105.9, 106.9, 122.9, 128.5, 129.0, 131.3, 132.9, 146.51, 161.7, 163.4, 164.8; MS (EI) m/z (%): 151(100), 167 (57), 182 (18), 269 (33), 349.1 (M$^+$, 5); 351.0 (M^{+2}, 5); I.R (KBr) υ_{max} (cm^{-1}): ArO-H: 3331, N-H: 3300, C-H-aromatic: 3046, C-H-aromatic: 3017, CH-aliphatic: 2970, CH-aliphatic: 2929, CH-aliphatic: 2839, C=O amide: 1654, C=N: 1593, C=C aromatic:1504, C=C aromatic:1488, C=C aromatic:1460, N-H: 1520, CH$_3$: 1384, CH$_3$:1256, C-H: 1361, C-N: 1203, C-O: 1156, C-Br: 633.

Synthesis of N′-(4-chlorobenzylidene)-2-hydroxy-4-methoxybenzohydrazide (4d)

White powder; yield: 58%; M.P: 210–214°C; ^{1}H NMR (500 MHz, DMSO-d_6) δ_H (ppm): 3.80 (s, 3H, OCH$_3$), 6.51 (d, J = 2.2 Hz, 1H, H$_3$-2-hydroxy-4-methoxy-N′-methylenebenzohydrazide), 6.56 (dd, J = 8.9, 2.2 Hz, 1H, H$_5$-2-hydroxy-4-methoxy-N′-methylenebenzohydrazide), 7.54 (d, J = 8.4 Hz, 2H, Ar-H), 7.77 (d, J = 8.2 Hz, 2H, Ar-H), 7.90 (d, J = 8.9 Hz, 1H, H$_6$-2-hydroxy-4-methoxy-N′-methylenebenzohydrazide), 8.45 (s, 1H, CH=N), 11.84 (s, 1H, OH), 12.45 (s, 1H, NH); ^{13}C NMR (126 MHz, DMSO) δ_c (ppm): 54.9, 100.8, 105.9, 106.9, 128.3, 128.4, 129.0, 132.6, 134.1, 146.4, 161.7, 163.4, 164.8; MS (EI), m/z (%): 151.0 (100), 166.9 (14), 304.7 (M$^+$, 10), 306.0(M^{+2}, 4); I.R (KBr) υ_{max} (cm^{-1}): ArO-H: 3331; N-H: 3327, C-H-aromatic: 3027, C-H-aromatic 3016,

CH-aliphatic: 2971, CH-aliphatic: 2931, C=O amide: 1656; C=N: 1593; C=C aromatic:1553, C=C aromatic: 1491, N-H: 1511, CH_3: 1362, C-N: 1258, C-O: 1156, C-Cl: 847.

Synthesis of 2-hydroxy-N′-(4-hydroxybenzylidene)-4-methoxybenzohydrazide (4e)

White crystal; yield: 41%; M.P: 215–220°C; ^1H NMR (500 MHz, DMSO-d_6) δ_H (ppm): 3.80 (s, 3H, OCH_3), 6.49 (d, J = 2.3 Hz, 1H, H_3-2-hydroxy-4-methoxy-N′-methylenebenzohydrazide), 6.55 (dd, J = 8.7, 2.3 Hz, 1H, H_5-2-hydroxy-4-methoxy-N′-methylenebenzohydrazide), 6.85 (d, J = 8.5 Hz, 2H, Ar-H), 7.58 (d, J = 8.5 Hz, 2H, Ar-H), 7.89 (d, J = 8.7 Hz, 1H, H_6-2-hydroxy-4-methoxy-N′-methylenebenzohydrazide), 8.36 (s, 1H, C=N), 10.00 (s, 1H, OH), 11.64 (s, 1H, OH), 12.66 (s, 1H, NH); ^{13}C NMR (126 MHz, DMSO) δ_c (ppm): 54.9, 100.8, 105.8, 106.8, 115.2, 124.5, 128.5, 128.7, 148.3, 159.1, 161.9, 163.3, 164.7; MS (EI), m/z (%): 151(100), 196.1(35), 286.1(M^+, 18); I.R(KBr) U_{max} (cm^{-1}): ArO-H: 3521, ArO-H: 3405, N-H: 3196, C-H-aromatic: 3024, CH-aliphatic: 2870, C=O amide: 1646, C=N: 1605, C=C aromatic: 1516, C=C aromatic: 1451, CH_3: 1377, C-H: 1304; C-N: 1223, C-O:1166.

Synthesis of 2-hydroxy-N′-(4-hydroxy-3,5-dimethoxybenzylidene)-4-methoxybenzohydrazide (4f)

Gray powder; Yield: 98%; M.P: 237–245°C; ^1H NMR (500 MHz, DMSO-d_6) δ_H (ppm): 3.80 (s, 3H, OCH_3), 3.83 (s, 6H, OCH_3), 6.49 (d, J = 2.2 Hz, 1H, H_3-2-hydroxy-4-methoxy-N′-methylenebenzohydrazide), 6.56 (dd, J = 8.9, 2.2 Hz, 1H, H_5-2-hydroxy-4-methoxy-N′-methylenebenzohydrazide), 7.01 (s, 2H, Ar-H), 7.90 (d, J = 8.9 Hz, 1H, H_6-2-hydroxy-4-methoxy-N′-methylenebenzohydrazide), 8.34 (s, 1H, Ar-H), 8.98 (s, 1H, N=CH), 11.68 (s, 1H, OH), 12.54 (s, 1H, NH); ^{13}C NMR (126 MHz, DMSO) δ_c (ppm): 54.9, 55.5, 100.8, 104.2, 105.8, 106.9, 123.8, 128.8, 137.6, 147.6, 148.5, 161.7, 163.3, 164.5; MS (EI), m/z (%): 151.0 (100), 180.1 (85), 330.1(28), 346.1 (M^+); I.R (KBr) U_{max} (cm^{-1}): ArO-H: 3521, ArO-H: 3434, N-H: 3227, C-H: aromatic: 3082, C-H: aromatic: 3059; CH-aliphatic: 2965, CH-aliphatic: 2942, CH-aliphatic: 2845, C=O amide: 1643, C=N: 1596, C=C aromatic: 1547, C=C aromatic: 1458, N-H: 1514, CH_3: 1377, C-N: 1228, C-O:1115.

Synthesis of N′-(3-ethoxy-4-hydroxybenzylidene)-2-hydroxy-4-methoxybenzohydrazide (4g)

White powder; Yield: 60%; M.P: 108–112°C; ^1H NMR (500 MHz, DMSO-d_6) δ_H (ppm): 1.37 (t, J = 6.9 Hz, 3H, CH_3, 2-ethoxyphenol), 3.80 (s, 3H, OCH_3), 4.07 (q, J = 6.9 Hz, 2H, 2-ethoxyphenol), 6.49 (d, J = 2.3 Hz, 1H, H_3-2-hydroxy-4-methoxy-N′-methylenebenzohydrazide), 6.55 (dd, J = 8.9, 2.3 Hz, 1H, H_5-2-hydroxy-4-methoxy-N′-methylenebenzohydrazide), 6.87 (d, J = 8.1 Hz, 1H, Ar-H), 7.11 (d, J = 8.9 Hz, 1H, Ar-H), 7.31 (s, 1H, Ar-H), 7.90 (d, J = 8.9 Hz, 1H, H_6-2-hydroxy-4-methoxy-N′-methylenebenzohydrazide), 8.34 (s, 1H, N=CH), 9.55 (s, 1H, OH), 11.65 (s, 1H, OH), 12.63 (s, 1H, NH); ^{13}C NMR (126 MHz, DMSO) δ_c (ppm): 14.2, 54.8, 63.3, 100.8, 105.8, 106.8, 109.7, 115.0, 121.7, 124.9, 128.7, 146.6, 148.5, 148.9, 161.8, 163.3, 164.6; MS (EI), m/z (%): 43(20), 89(23), 151.0(100), 193(14), 207 (5), 330.1 (M^+, 18); I.R (KBr) U_{max} (cm^{-1}): ArO-H: 3524, N-H: 3301, C-H-aromatic: 3080, CH-aliphatic: 2975, CH-

aliphatic: 2845, C=O amide: 1637, C=N: 1589, C=C aromatic:1504, C=C aromatic: 1444, N-H: 1520, CH_3:1371, C-N: 1200, C-O:1155.

Synthesis of 2-hydroxy-N′-(3-hydroxy-4-methoxybenzylidene)-4-methoxybenzohydrazide (4h)

White powder; Yield: 54%; M.P: 236–240°C; ^1H NMR (500 MHz, DMSO-d_6) δ_H (ppm): 3.80 (s, 3H, OCH_3), 3.82 (s, 3H, OCH_3), 6.50 (d, J = 2.6 Hz, 1H, H_3-2-hydroxy-4-methoxy-N′-methylenebenzohydrazide), 6.55 (dd, J = 9.0, 2.6 Hz, 1H, H_5-2-hydroxy-4-methoxy-N′-methylenebenzohydrazide), 6.98 (d, J = 8.3 Hz, 1H, Ar-H), 7.09 (dd, J = 8.4, 2.0 Hz, 1H, Ar-H), 7.30 (d, J = 2.1 Hz, 1H, Ar-H), 7.89 (d, J = 9 Hz, 1H, H_6-2-hydroxy-4-methoxy-N′-methylenebenzohydrazide), 8.32 (s, 1H, Ar-H), 9.36 (s, 1H, N=CH), 11.65 (s, 1H, OH), 12.63 (s, 1H, NH); ^{13}C NMR (126 MHz, DMSO) δ_c (ppm): 54.9, 55.0, 100.8, 105.8, 106.8, 111.3, 111.8, 119.9, 126.4, 128.7, 146.3, 148.1, 149.4, 161.9, 163.3, 164.70; MS (EI), m/z (%): 151.0 (100), 167 (9), 301 (10), 316.0 (M^+, 12); I.R (KBr) U_{max} (cm^{-1}): ArO-H: 3390, N-H: 3316, C-H-aromatic: 3087, CH-aliphatic: 2992, CH-aliphatic: 2949, CH-aliphatic: 2915, CH-aliphatic: 2838, C=O amide: 1642, C=N: 1598, C=C aromatic: 1555, C=C aromatic:1440, N-H: 1503, CH_3:1326, C-N: 1212, C-O:1108.

Synthesis of N′-(3,4-dimethoxybenzylidene)-2-hydroxy-4-methoxybenzohydrazide (4i)

White powder; Yield: 90%; M.P: 162–167°C; ^1H NMR (500 MHz, DMSO-d_6) δ_H (ppm): 3.85–3.79 (m, 9H, OCH_3), 6.50 (d, J = 2.3 Hz, 1H, H_3-2-hydroxy-4-methoxy-N′-methylenebenzohydrazide), 6.55 (dd, J = 8.8, 2.3 Hz, 1H, H_5-2-hydroxy-4-methoxy-N′-methylenebenzohydrazide), 7.04 (d, J = 8.3 Hz, 1H, Ar-H), 7.23 (d, J = 8.2 Hz, 1H, Ar-H), 7.36 (s, 1H, Ar-H), 7.90 (d, J = 8.8 Hz, 1H, H_6-2-hydroxy-4-methoxy-N′-methylenebenzohydrazide), 8.39 (s, 1H, N=CH), 11.66 (s, 1H, OH), 12.53 (s, 1H, NH); ^{13}C NMR (126 MHz, DMSO) δ_c (ppm): 54.9, 54.9, 55.0, 100.7, 105.8, 106.9, 107.8, 110.9, 121.5, 126.3, 128.8, 148.1, 148.5, 150.4, 161.8, 163.3, 164.7; MS (EI), m/z (%): 151.0 (100), 315 (10), 330.1 (M^+, 15); I.R (KBr) U_{max} (cm^{-1}): ArO-H: 3313, N-H: 3293, C-H-aromatic: 3077, C-H-aromatic: 3009, CH-aliphatic: 2964, CH-aliphatic: 2935, CH-aliphatic: 2916, C=O amide: 1639, C=N: 1597, N-H: 1556, C=C aromatic: 1513, C=C aromatic: 1461, CH_3: 1367, C-H: 1361, C-N: 1258, C-O: 1168.

Synthesis of N′-(4-acetyl-3-methoxybenzylidene)-2-hydroxy-4-methoxybenzohydrazide (4j)

White powder; Yield: 42%; M.P: 180–185°C; ^1H NMR (500 MHz, DMSO-d_6) δ_H (ppm): 2.29 (s, 3H, C=O-CH_3), 3.81 (s, 3H, OCH_3), 3.85 (s, 3H, OCH_3), 6.51 (d, J = 2.3 Hz, 1H, H_3-2-hydroxy-4-methoxy-N′-methylenebenzohydrazide), 6.57 (dd, J = 8.9, 2.3 Hz, 1H, H_5-2-hydroxy-4-methoxy-N′-methylenebenzohydrazide), 7.20 (d, J = 8.0 Hz, 1H, Ar-H), 7.32 (d, J = 8.9 Hz, 1H, H_6-2-hydroxy-4-methoxy-N′-methylenebenzohydrazide), 7.48 (s, 1H, Ar-H), 7.91 (d, J = 8.7 Hz, 1H, Ar-H), 8.45 (s, 1H, N=CH), 11.83 (s, 1H, OH), 12.51 (s, 1H, NH); ^{13}C NMR (126 MHz, DMSO) δ_c (ppm): 19.8, 54.9, 55.3, 100.8, 105.9, 106.9, 109.4, 120.1, 122.8, 129.0, 132.5, 140.4, 147.2, 150.7, 161.7, 163.4, 164.7, 167.9; MS (EI), m/z (%): 57.1(33), 149.0 (100), 152 (74), 192.2 (95), 342.3 (M^+, 20); I.R (KBr) U_{max} (cm^{-1}):

ArO-H: 3582, 3582, 3534, N-H: 3300, C-H-aromatic: 3092, C-H-aromatic: 3049, CH-aliphatic: 2975, CH-aliphatic: 2952, CH-aliphatic: 2855, C=O ketone: 1675, C=O amide: 1653, C=N: 1595, C=C aromatic: 1547, C=C aromatic: 1458, N-H: 1514, CH_3:1357, C-N: 1228, C-O: 1115.

2.2 | Tyrosinase inhibition assay

The anti-tyrosinase activity was performed using L-dopa as a substrate. All the assays were under 50 mM M KH_2PO_4/K_2HPO_4 buffer, pH 6.8, in 200 μL total volume using commercially available tyrosinase (EC 1.14.18.1, 5771 units/mg solid). At first, 160 μL phosphate buffer was added to each well of 96-well polystyrene photometric microplates and then 10 μL tyrosinase (0.5 mg/ml) was added to wells. Ten microliters of the compounds at different concentrations (prepared in DMSO) was added to the test well and preincubated for 20 min. Finally, 20 μL of the L-dopa solution as substrate was added and the absorbance was measured at 475 nm using a microplate reader. For the positive control, tested compounds were replaced with a positive drug. In the blank group, 190 μL phosphate buffer was added without positive control or tested derivatives and substrate. Each group was measured three times in parallel to average. The IC_{50} values of the compounds showing half of the maximal inhibitory concentration, the measurements and the calculations were determined with GraphPad Prism 6. Results were expressed as mean ± SE and all experiments were performed in triplicate.
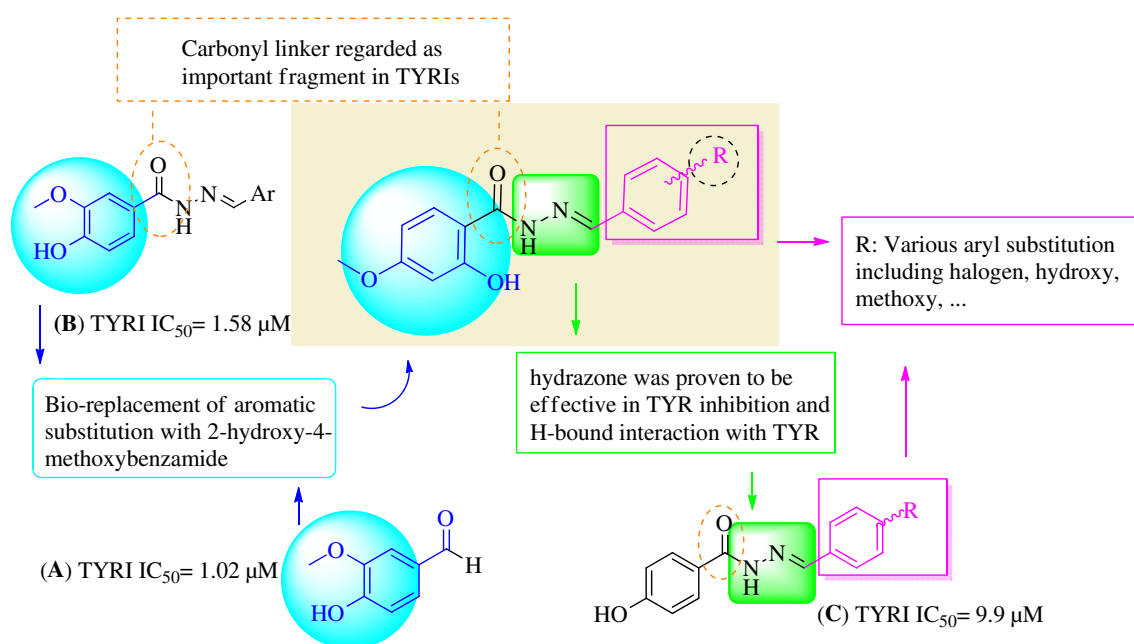
FIGURE 1 Design of new 2-hydroxy-4-methoxybenzohydrazide analogs
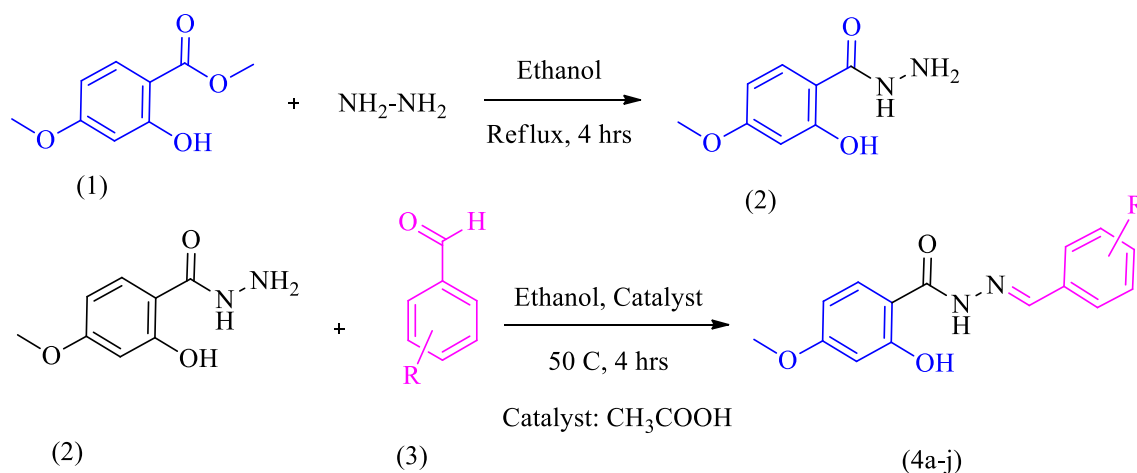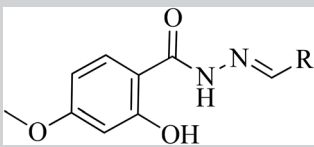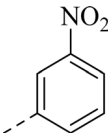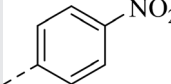
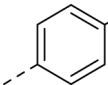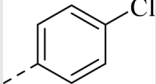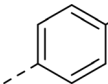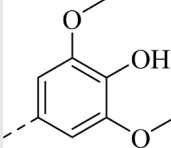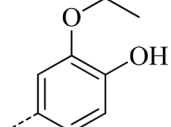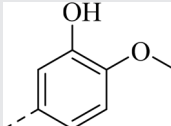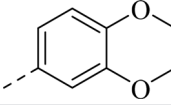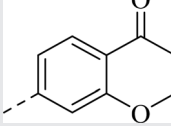**SCHEME 1** Synthesis of N′-benzylidene-2-hydroxy-4-methoxybenzohydrazide derivatives **4a–j**

2.3 | Kinetic assay

The mechanism of action of **4d** was obtained by Lineweaver–Burk plot in which the reaction rate and substrate concentration were used to determine the type of inhibition of the TYRI by the mentioned compound. Compound **4d** at several concentrations was added to the assay solution containing various concentrations of L-dopa (0.1, 0.25, 0.5, 0.75, and 1.5 mM) as the substrate and pre-incubated with the enzyme at 37 °C for 20 min. Kinetic characterization catalyzed by enzymes was achieved spectrometrically at 475 nm. The obtained data including michaelis constant (K_m) and the maximal velocity (V_{max}) were transformed to Lineweaver–Burk

TABLE 1 Chemical structures and physical properties of the synthesized compounds

Compound	Chemical formula	R	Yield (%)[a]	Melting point[a]
4a	$C_{15}H_{13}N_3O_5$		92	260–264
4b	$C_{15}H_{13}N_3O_5$		54	264–266
4c	$C_{15}H_{13}BrN_2O_3$		57	224–227
4d	$C_{15}H_{13}ClN_2O_3$		58	210–214
4e	$C_{15}H_{14}N_2O_4$		41	215–220
4f	$C_{17}H_{18}N_2O_6$		98	241–245
4g	$C_{17}H_{18}N_2O_5$		60	108–112
4h	$C_{16}H_{16}N_2O_5$		54	236–240
4i	$C_{17}H_{18}N_2O_5$		90	162–167
4j	$C_{18}H_{18}N_2O_5$		42	180–185

[a]Yield of isolated purified compounds.

plots of the inverse of velocities (1/V) versus the inverse of substrate concentrations 1/[S] mM.

2.4 | Molecular docking

The molecular docking studies were performed with the Autodock 4.2package with the pymol program. The crystal structure of tyrosinase (PDB code: 2Y9X) was downloaded from the RCSB protein data bank and prepared with Autodock 4.2 package. Briefly, water molecules were removed, missing hydrogens and residues were added, nonpolar hydrogens were merged and Gasteiger charges were calculated for protein. The glide grid center was setting according the geometrical center of the original inhibitor (tropolone) and the grid size was $60 \times 60 \times 60$ A$^{\circ 3}$ with the default grid spacing of 0.375 A$^\circ$. The other parameters were left at program default values. The 3D structures of the ligands were drawn by using the ChemDraw software, minimized energy using semiempirical force field and prepared using the LigPrep platform. Lamarckian genetic algorithm was applied to model the interaction/binding between then ligand and the tyrosinase active site. To choose and validate the docking algorithm, the tropolone as cognate ligand inside the 2Y9X was redocked. Finally, the best docking confirmations with minimum binding energy were visualized using Discovery studio (Edraki et al., 2015).
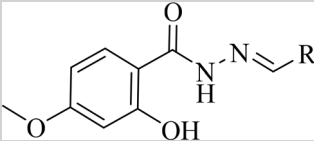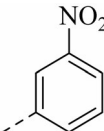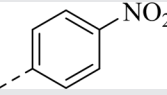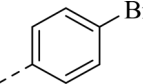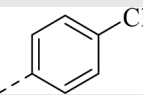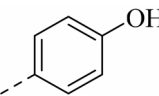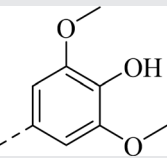
3 | RESULTS AND DISCUSSION

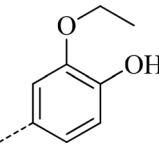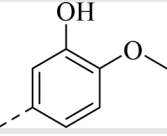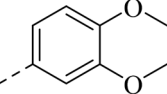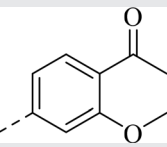### 3.1 | Design of novel 2-hydroxy-4-methoxybenzamide derivatives

Literature survey highlighted natural and synthetic TYRIs including terpenoids (Ashraf et al., 2017; Lehbili et al., 2018; Revoltella et al., 2019) chalcones, hydrochalcones (Huang et al., 2010; Niesen et al., 2015; Takahashi et al., 2012), oxadiazole, triazolothiadiazole (Ghani & Ullah, 2010; Ha et al., 2012; Lam et al., 2010), thiosemicarbazone (Lee et al., 2010; Yi et al., 2011) derivatives. Among them phenolic contacting structures exerted the stimulating anti-TYR properties with low toxicity by forming compound-Cu^{2+}-histidine complex.

- In previous studies, 4-hydroxy-3-methoxy benzaldehyde analogs (compounds **A** and **B**, Figure 1) demonstrated promising anti-tyrosinase activity (Iraji et al., 2020; Walton et al., 2003). In this study 2-hydroxy-4-methoxybenzaldehyde as the core backbone was selected due to potential binding ability to TYR enzymes via strong hydrogen bond interactions using OH and OCH$_3$ motifs. Moreover, the benzene aromatic ring could exert weak interactions such as ion-dipole, Van der Waals force, and so on.
- Carbonyl-based compounds and related analogs (compound **C**, Figure 1) are known by their copper chelating ability (Iraji et al., 2018; Iraji et al., 2019) and H-bond interactions with amino

TABLE 2 IC$_{50}$ values of N′-benzylidene-2-hydroxy-4-methoxybenzohydrazide against tyrosinase enzyme in the presence of L-dopa as the substrate

Compounds	R	IC$_{50}$ (µM)[a]
4a		9.43 ± 0.43
4b		8.19 ± 0.25
4c		10.01 ± 0.52
4d		7.57 ± 0.01
4e		56.05 ± 0.71
4f		50.10 ± 0.68
4g		10.0 ± 0.56
4h		81.25 ± 1.15
4i		9.20 ± 0.18
4j		8.92 ± 0.016
Kojic acid[b]	–	20.24 ± 4.28

[a]Data presented here are the mean ± *SEM*. of three to six independent experiments.
[b]Used as positive control.

acids in TYR, leading to inactivation and loss of proteins function as efficient anti-TYR agents.

- Hydrazone linker (compounds **B** and **C**, Figure 1) as an active nucleophilic motif could covalently bind to electron-deficient groups; therefore, various aryl groups could bind into hydrazone linker to investigate the effects of substitutions on TYR inhibitory activities. Furthermore, hydrazone linker also exerts a pivotal role *via* H-bound interactions with a TYR enzyme (Dehghani et al., 2019; Iraji et al., 2019; Iraji et al., 2020).

As a result, the newly prepared 2-hydroxy-4-methoxybenzohydrazide analogs were designed and screened for their in vitro anti-tyrosinase activities. Mechanism of inhibition and molecular docking studies of the highly active compound was also evaluated.

3.2 | Chemistry

An efficient synthesis of the new N′-benzylidene-2-hydroxy-4-methoxybenzohydrazide analogs **4a-j** has been performed starting with methyl 2-hydroxy-4-methoxybenzoate (1) according to literature methods (Schemes 1.).

Commercially available methyl 2-hydroxy-4-methoxybenzoate (**1**, Schemes 1) was reacted with hydrazine hydrate *via* nucleophilic substitution reaction in refluxing ethanol to produce intermediate **2** in an excellent yield of 83%. Intermediate **2** was stirred with catalytic amounts of acetic acid in refluxing ethanol and then substituted aromatic aldehydes were added to the mixture. Completion of the reaction was monitored by TLC. Then, the mixture was concentrated and the obtained precipitate was filtered and crystallized from ethanol. ^{1}H and ^{13}C NMR confirmed all the hydrogen and carbon atoms of the synthesized compounds. Mass spectroscopy confirmed the molecular weights of compounds by their molecular ion peaks. Some physical properties of synthesized derivatives are presented in Table 1.

3.3 | Structure–activity relationship studies

The synthesized compounds (**4a–j**) were evaluated for their anti-TYR potential against mushroom TYR. The concentrations of compounds required for 50% inhibition of TYR enzyme (IC$_{50}$) were determined and listed in Tables 2.

All the compounds exhibited moderate to significant anti-TYR activity with IC$_{50}$ values ranging from 7.57 to 81.25 μM compared to standard drug Kojic acid with IC$_{50}$ = 20.24 ± 4.28 μM.

According to these data, the preliminary SARs of these novel N′-benzylidene-2-hydroxy-4-methoxybenzohydrazide derivatives were summarized in Figure 2.

1. The activities comparison of compounds **4a** and **4b** containing NO$_2$ motif demonstrated that 4-NO$_2$ substitution (**4b**, IC$_{50}$ = 8.19 ± 0.25 μM) had better potency than 3-NO$_2$ one (**4a**, IC$_{50}$ = 9.43 ± 0.43 μM).
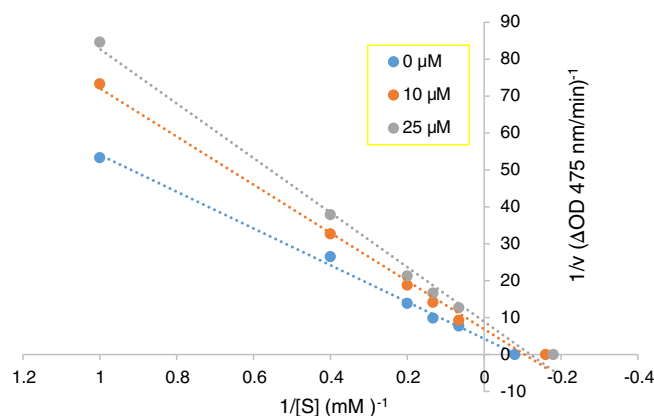2. The inhibitory activity of synthetic derivatives depicted that **4d** (*para*-chlorinated compound) was the best TYRI with IC$_{50}$ of

FIGURE 3 Lineweaver–Burk plot obtained through the kinetics study of the compound **4d** on TYR
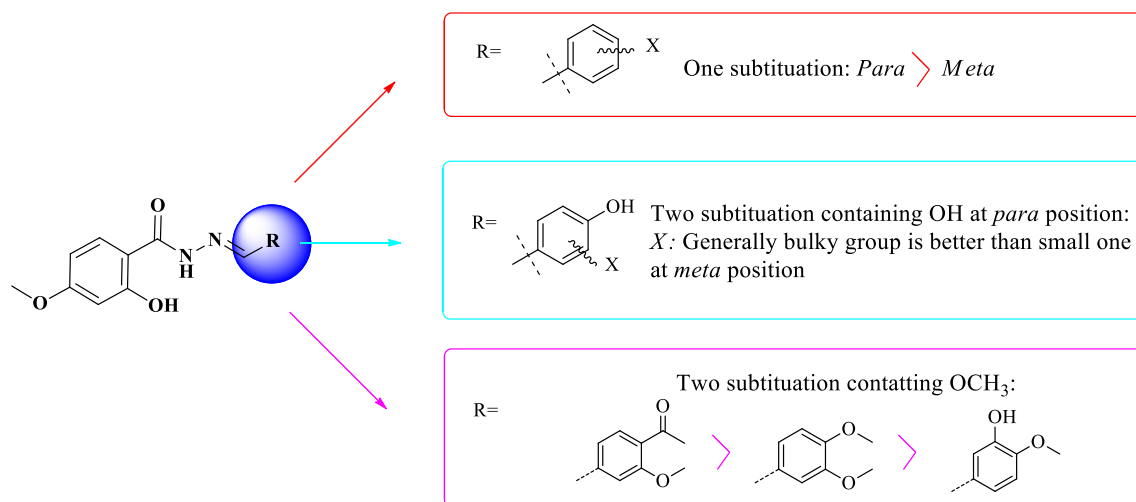
FIGURE 2 General representation of 2-hydroxy-4-methoxybenzamide for SAR analysis

7.57 μM. It seems that the *para* substituent on the benzyl ring is crucial to improve the anti-TYR activities.

3. The effects of OH motif on the benzyl ring were also considered. Compound **4e** with the 4-OH-benzyl group at R position depicted the IC$_{50}$ of 56.05 μM. Adding two extra methoxy groups with electron-donating properties slightly increases the inhibitory activity like **4f** with IC$_{50}$ of 50.10 μM. Interestingly, compounds **4g** with 4-hydroxy-3-ethoxybenzyl motif at R position demonstrated significant improvement against tyrosinase (IC$_{50}$ = 10.0 ± 0.56 μM). This might be attributed to the presence of extra bulky sites of hydrogen bonding interaction in **4g** with TYR.

4. In the case of OMe-substituted compounds (**4f**, **4h**, **4i**, and **4j**), it was found that the least activity belong to **4h** with 3-hydroxy-4-methoxy benzyl derivative at R position. Unexpectedly, the isosteric substitution of a *meta*-OH group with a *meta*-OMe substituent of phenyl ring can increase the inhibitory activity significantly (**4h**, IC$_{50}$ = 81.25 ± 1.15 μM vs. **4i**, IC$_{50}$ = 9.20 ± 0.18 μM). The replacement of *para* methoxy group of **4i** with acetyl one exerted another excellent TYR inhibitor (**4j**) with IC$_{50}$ of 8.92 μM. These data were contributed to the anti-tyrosinase activities of OMe-containing compounds in the order of **4j** (3-methoxy,4-hydroxy) > **4i** (3,4-dimethoxy) > **4f** (4-hydroxy-3,5-dimethoxy) > **4h** (3-hydroxy, 4-methoxy) analogs.

3.4 | The mechanism of tyrosine inhibition

A study for the inhibitory mechanism of action was carried out with the active TYRI compound, **4d**. For this purpose, the rate of the enzyme activity was carried out without the inhibitor and in 10 and 20 μM concentrations of the inhibitor in the presence of tyrosinase enzyme using different concentrations of L-dopa as substrate (0.25,

0.5, 0.75, and 1 mM). A parallel control experiment was carried out without compound **4d** in the mixture. Lineweaver–Burk plot was made based on the reaction rate and substrate concentration to determine the type of inhibition of the TYR by the compound. The graphical analysis and inhibitory data of the **4d** against TYR is shown in Figure 3 and Table 3, respectively. According to the Figure 3, it can be judged that the inhibition mode of compound **4d** against TYR is mixed inhibition.

3.5 | Molecular modeling

With the aim of obtaining useful information about the binding interactions between the most potent compound (**4d**) and inactive compound (**4h**) molecular modeling study was carried out using a docking program AUTODOCK 4.0 package with PyMOL program. The free binding energy of the mentioned compounds plus their interactions with amino acid residues in the TYR active site were presented in Table 4. The self-docking validation process resulted in RMSD <2.0.

3D interaction patterns of compound **4d** have been shown in Figure 4. Compound **4d** as the most potent TYR inhibitor with IC$_{50}$ value 7.57 μM demonstrated critical metal acceptor interaction with one of Cu^{2+} ion plus H-bound and pi-pi interactions with His263. Further four π-aryl stacking interactions were also constructed which

TABLE 3 Kinetic parameters for the compounds **4d** against TYR

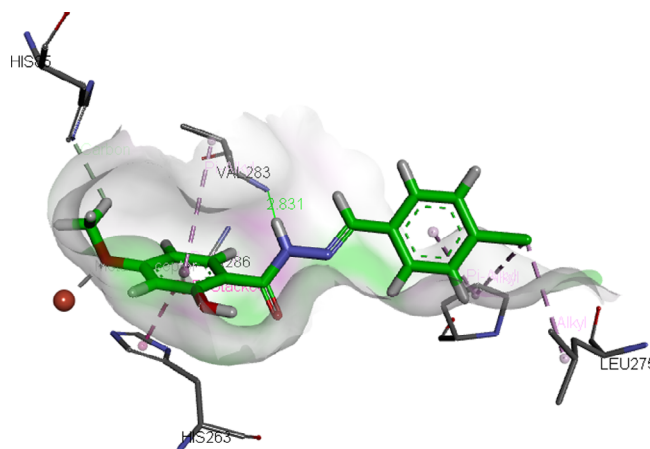| Compound	K_m (mM)	V_m (OD/min)
4d (0 μM)	11.64	0.23
4d (10 μM)	12.18	0.22
4d (25 μM)	12.91	0.21

FIGURE 4 3D interaction pattern of **4d** in the active site of TYR enzyme

TABLE 4 Docking scores and interactions of **4d** and **4h** against TYR enzyme

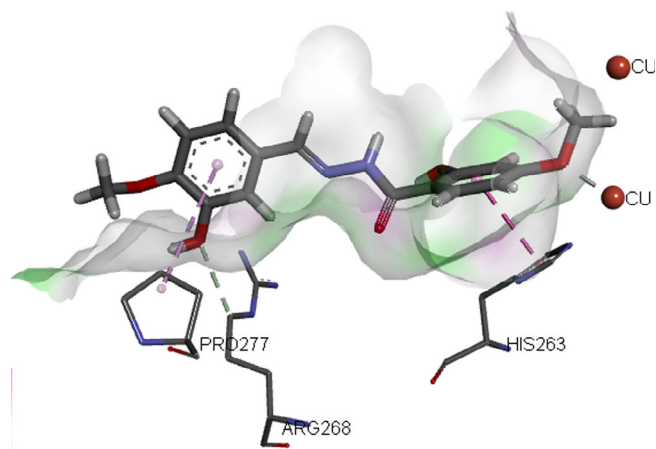| Compound	ΔG_b (kcal/Mol)	K_i	Interactions
4d	−9.95	50.75 (nM)	Hydrogen bond: Val283 Pi-pi interaction: His263 Pi-Aryl interaction: Val283 Pi-Aryl interaction: Ala286 Pi-Aryl interaction: Pro277 Pi-Aryl interaction: Lue275 Metal acceptor interactions: one Cu^{2+}
4h	−6.71	12.06 (μM)	Pi-Aryl interaction: Pro277 Pi-pi interactions: His263 Metal acceptor interactions: one Cu^{2+}

FIGURE 5 3D interaction pattern of **4h** in the active site of TYR enzyme

justify low binding energy and high potency of this synthetic compound against TYR. As depicted in Figure 5, compound **4h** as the least active compound (IC$_{50}$ = 81.25 ± 1.15 μM) showed one metal acceptor interaction with copper ion and two der Waals interactions between the aromatic core of **4h** and Pro277 and His263. The absence of a hydrogen bond with critical residue of TYR active site confirmed the lower binding capability of **4h** and lower *in vitro* potency.

4 | CONCLUSION

In conclusion, a structure-based drug design allowed us to synthesize a series of novel N′-benzylidene-2-hydroxy-4-methoxybenzohydrazide derivatives. Some of the synthesized conjugates exhibited enhanced anti-TYR properties with potency higher than that of standard kojic acid as reference. Among them, compound **4d** (R = *para* chlorobenzyl) was found to be a highly potent compound with IC$_{50}$ value of 7.57 μM followed by **4b** containing *para* nitrobenzyl (IC$_{50}$ = 8.19 ± 0.25 μM). The SARs depicted the presence of *para* substitution significantly enhanced anti-TYR activities. Based on molecular docking study, the ability of **4d** to make pi-pi and H-bonds interactions with important histidine and Cu-acceptor within TYR active site effectively justify high potency of this compound. It was worth noting that **4d** demonstrated mixed inhibition in enzymatic assay. Finally, the results indicated that these new compounds could be considered as a new lead for further optimization.

CONFLICT OF INTEREST

The authors declare that they have no competing interests.

ORCID

Aida Iraji https://orcid.org/0000-0002-8442-2205
Zahra Panahi https://orcid.org/0000-0002-4967-1361
Najmeh Edraki https://orcid.org/0000-0001-8306-2642
Mahsima Khoshneviszadeh https://orcid.org/0000-0002-6993-4624
Mehdi Khoshneviszadeh https://orcid.org/0000-0003-1458-2964

REFERENCES

Ashraf, Z., Rafiq, M., Nadeem, H., Hassan, M., Afzal, S., Waseem, M., … Latip, J. (2017). Carvacrol derivatives as mushroom tyrosinase inhibitors; synthesis, kinetics mechanism and molecular docking studies. *PLoS One*, *12*(5), e0178069. https://doi.org/10.1371/journal.pone.0178069.

Choi, J., Park, S.-J., & Jee, J.-G. (2015). Analogues of ethionamide, a drug used for multidrug-resistant tuberculosis, exhibit potent inhibition of tyrosinase. *European Journal of Medicinal Chemistry*, *106*, 157–166. https://doi.org/10.1016/j.ejmech.2015.10.033.

Dehghani, Z., Khoshneviszadeh, M., Khoshneviszadeh, M., & Ranjbar, S. (2019). Veratric acid derivatives containing benzylidene-hydrazine moieties as promising tyrosinase inhibitors and free radical scavengers. *Bioorganic & Medicinal Chemistry*, *27*(12), 2644–2651. https://doi.org/10.1016/j.bmc.2019.04.016.

Edraki, N., Firuzi, O., Fatahi, Y., Mahdavi, M., Asadi, M., Emami, S., … Foroumadi, A. (2015). N-(2-[Piperazin-1-yl]phenyl)arylamide derivatives as β-Secretase (BACE1) inhibitors: Simple synthesis by Ugi four-component reaction and biological evaluation. *Archiv der Pharmazie*, *348*(5), 330–337. https://doi.org/10.1002/ardp.201400322.

Ghani, U., & Ullah, N. (2010). New potent inhibitors of tyrosinase: Novel clues to binding of 1, 3, 4-thiadiazole-2 (3H)-thiones, 1, 3, 4-oxadiazole-2 (3H)-thiones, 4-amino-1, 2, 4-triazole-5 (4H)-thiones, and substituted hydrazides to the dicopper active site. *Bioorganic & Medicinal Chemistry*, *18*(11), 4042–4048.

Ha, Y. M., Park, Y. J., Lee, J. Y., Park, D., Choi, Y. J., Lee, E. K., … Lee, H. J. (2012). Design, synthesis and biological evaluation of 2-(substituted phenyl) thiazolidine-4-carboxylic acid derivatives as novel tyrosinase inhibitors. *Biochimie*, *94*(2), 533–540.

Hałdys, K., & Latajka, R. (2019). Thiosemicarbazones with tyrosinase inhibitory activity. *MedChemComm*, *10*(3), 378–389.

Huang, W. Y., Cai, Y. Z., & Zhang, Y. (2010). Natural phenolic compounds from medicinal herbs and dietary plants: Potential use for cancer prevention. *Nutrition and Cancer*, *62*(1), 1–20. https://doi.org/10.1080/01635580903191585.

Iraji, A., Adelpour, T., Edraki, N., Khoshneviszadeh, M., Miri, R., & Khoshneviszadeh, M. (2020). Synthesis, biological evaluation and molecular docking analysis of vaniline–benzylidenehydrazine hybrids as potent tyrosinase inhibitors. *BMC Chemistry*, *14*(1), 28. https://doi.org/10.1186/s13065-020-00679-1.

Iraji, A., Firuzi, O., Khoshneviszadeh, M., Nadri, H., Edraki, N., & Miri, R. (2018). Synthesis and structure-activity relationship study of multi-target triazine derivatives as innovative candidates for treatment of Alzheimer's disease. *Bioorganic Chemistry*, *77*, 223–235. https://doi.org/10.1016/j.bioorg.2018.01.017.

Iraji, A., Khoshneviszadeh, M., Bakhshizadeh, P., Edraki, N., & Khoshneviszadeh, M. (2019). Structure-based design, synthesis, biological evaluation and molecular docking study of 4-Hydroxy-N'-methylenebenzohydrazide derivatives acting as Tyrosinase inhibitors

as potentiate anti-Melanogenesis activities. *Medicinal Chemistry*, *16*(7), 892–902. https://doi.org/10.2174/1573406415666190724142951.

Ismaya, W. T., Rozeboom, H. J., Weijn, A., Mes, J. J., Fusetti, F., Wichers, H. J., & Dijkstra, B. W. (2011). Crystal structure of Agaricus bisporus mushroom tyrosinase: Identity of the tetramer subunits and interaction with tropolone. *Biochemistry*, *50*(24), 5477–5486.

Khoshneviszadeh, M., Ghahremani, M. H., Foroumadi, A., Miri, R., Firuzi, O., Madadkar-Sobhani, A., … Shafiee, A. (2013). Design, synthesis and biological evaluation of novel anti-cytokine 1,2,4-triazine derivatives. *Bioorganic & Medicinal Chemistry*, *21*(21), 6708–6717. https://doi.org/10.1016/j.bmc.2013.08.009.

Lam, K. W., Syahida, A., Ul-Haq, Z., Rahman, M. B. A., & Lajis, N. H. (2010). Synthesis and biological activity of oxadiazole and triazolothiadiazole derivatives as tyrosinase inhibitors. *Bioorganic & Medicinal Chemistry Letters*, *20*(12), 3755–3759.

Lavezzo, M. M., Sakata, V. M., Morita, C., Rodriguez, E. E. C., Abdallah, S. F., da Silva, F. T., … Yamamoto, J. H. (2016). Vogt-Koyanagi-Harada disease: Review of a rare autoimmune disease targeting antigens of melanocytes. *Orphanet Journal of Rare Diseases*, *11*(1), 29.

Lee, K.-C., Thanigaimalai, P., Sharma, V. K., Kim, M.-S., Roh, E., Hwang, B.-Y., … Jung, S.-H. (2010). Structural characteristics of thiosemicarbazones as inhibitors of melanogenesis. *Bioorganic & Medicinal Chemistry Letters*, *20*(22), 6794–6796.

Lehbili, M., Alabdul Magid, A., Hubert, J., Kabouche, A., Voutquenne-Nazabadioko, L., Renault, J.-H., … Kabouche, Z. (2018). Two new bis-iridoids isolated from Scabiosa stellata and their antibacterial, antioxidant, anti-tyrosinase and cytotoxic activities. *Fitoterapia*, *125*, 41–48. https://doi.org/10.1016/j.fitote.2017.12.018.

Loizzo, M., Tundis, R., & Menichini, F. (2012). Natural and synthetic tyrosinase inhibitors as antibrowning agents: An update. *Comprehensive Reviews in Food Science and Food Safety*, *11*(4), 378–398.

Matoba, Y., Kumagai, T., Yamamoto, A., Yoshitsu, H., & Sugiyama, M. (2006). Crystallographic evidence that the dinuclear copper center of tyrosinase is flexible during catalysis. *Journal of Biological Chemistry*, *281*(13), 8981–8990.

Neagu, E., Radu, G. L., Albu, C., & Paun, G. (2018). Antioxidant activity, acetylcholinesterase and tyrosinase inhibitory potential of Pulmonaria officinalis and Centarium umbellatum extracts. *Saudi Journal of Biological Sciences*, *25*(3), 578–585.

Niesen, D. B., Ma, H., Yuan, T., Bach, A. C., 2nd, Henry, G. E., & Seeram, N. P. (2015). Phenolic constituents of *Carex vulpinoidea* seeds and their tyrosinase inhibitory activities. *Natural Product Communications*, *10*(3), 491–493.

Piechowska, K., Świtalska, M., Cytarska, J., Jaroch, K., Łuczykowski, K., Chałupka, J., … Kruszewski, S. (2019). Discovery of tropinone-thiazole derivatives as potent caspase 3/7 activators, and noncompetitive tyrosinase inhibitors with high antiproliferative activity: Rational design, one-pot tricomponent synthesis, and lipophilicity determination. *European Journal of Medicinal Chemistry*, *175*, 162–171.

Revoltella, S., Rainer, B., Waltenberger, B., Pagitz, K., Schwaiger, S., & Stuppner, H. (2019). HPTLC autography based screening and isolation of mushroom Tyrosinase inhibitors of European plant species. *Chemistry & Biodiversity*, *16*(3), e1800541.

Singh, B., Suri, K., Shevkani, K., Kaur, A., Kaur, A., & Singh, N. (2018). Enzymatic browning of fruit and vegetables: A review. In *Enzymes in food technology* (pp. 63–78). Springer.

Takahashi, M., Takara, K., Toyozato, T., & Wada, K. (2012). A novel bioactive chalcone of Morus australis inhibits tyrosinase activity and melanin biosynthesis in B16 melanoma cells. *Journal of Oleo Science*, *61*(10), 585–592.

Walton, N. J., Mayer, M. J., & Narbad, A. (2003). Vanillin. *Phytochemistry*, *63*(5), 505–515. https://doi.org/10.1016/S0031-9422(03)00149-3.

Yazdani, M., Edraki, N., Badri, R., Khoshneviszadeh, M., Iraji, A., & Firuzi, O. (2019). Multi-target inhibitors against Alzheimer disease derived from 3-hydrazinyl 1,2,4-triazine scaffold containing pendant phenoxy methyl-1,2,3-triazole: Design, synthesis and biological evaluation. *Bioorganic Chemistry*, *84*, 363–371. https://doi.org/10.1016/j.bioorg.2018.11.038.

Yi, W., Dubois, C., Yahiaoui, S., Haudecoeur, R., Belle, C., Song, H., … Boumendjel, A. (2011). Refinement of arylthiosemicarbazone pharmacophore in inhibition of mushroom tyrosinase. *European Journal of Medicinal Chemistry*, *46*(9), 4330–4335.

Yuan, Y., Jin, W., Nazir, Y., Fercher, C., Blaskovich, M. A. T., Cooper, M. A., … Ziora, Z. M. (2020). Tyrosinase inhibitors as potential antibacterial agents. *European Journal of Medicinal Chemistry*, *187*, 111892. https://doi.org/10.1016/j.ejmech.2019.111892.

Zolghadri, S., Bahrami, A., Hassan Khan, M. T., Munoz-Munoz, J., Garcia-Molina, F., Garcia-Canovas, F., & Saboury, A. A. (2019). A comprehensive review on tyrosinase inhibitors. *Journal of Enzyme Inhibition and Medicinal Chemistry*, *34*(1), 279–309.

SUPPORTING INFORMATION

Additional supporting information may be found online in the Supporting Information section at the end of this article.